Miniature and Tunable Filters Using MEMS Capacitors

Abbas Abbaspour-Tamijani, *Student Member, IEEE*, Laurent Dussopt, *Member, IEEE*, and Gabriel M. Rebeiz, *Fellow, IEEE*

***Abstract*—Microelectromechanical system (MEMS) bridge capacitors have been used to design miniature and tunable bandpass filters at 18–22 GHz. Using coplanar waveguide transmission lines on a quartz substrate ($\varepsilon_r = 3.8$, $\tan\delta = 0.0002$), a miniature three-pole filter was developed with 8.6% bandwidth based on high-Q MEMS bridge capacitors. The miniature filter is approximately 3.5 times smaller than the standard filter with a midband insertion loss of 2.9 dB at 21.1 GHz. The MEMS bridges in this design can also be used as varactors to tune the passband. Such a tunable filter was made on a glass substrate ($\varepsilon_r = 4.6$, $\tan\delta = 0.006$). Over a tuning range of 14% from 18.6 to 21.4 GHz, the miniature tunable filter has a fractional bandwidth of 7.5 $\pm$ 0.2% and a midband insertion loss of 3.85–4.15 dB. The IIP_3 of the miniature-tunable filter is measured at 32 dBm for the difference frequency of 50 kHz. The IIP_3 increases to $>$50 dBm for difference frequencies greater than 150 kHz. Simple mechanical simulation with a maximum dc and ac (ramp) tuning voltages of 50 V indicates that the filter can tune at a conservative rate of 150–300 MHz/μs.**

***Index Terms*—Filters, microelectromechanical system (MEMS), MEMS varactors, MEMS devices, miniature filters, tunable filters.**

I. Introduction

LOW-LOSS bandpass filters are the basic components of transceivers, either as band-select or image-reject units. In the highly integrated systems, however, design of the bandpass filters is generally subject to serious size constraints. In active phased arrays, for example, one filter is required per antenna element, and the filter size cannot exceed a fraction of the free-space wavelength, which is the typical cell size in the array. Also, in multiband receivers, a single filter cannot fulfill the filtering requirements for all operating bands and multiple filters must be used, which proves inconvenient in most communication systems.

An ideal solution in such circumstances is a miniature filter that can be tuned for different bands. The existing work in the area of filter miniaturization includes loading of the transmission-line resonators with lumped elements [1], [2], novel compact geometry resonators [3]–[6], dual-mode resonators [7]–[10], and using new materials and artificial dielectrics [5], [11]–[13]. Among these, the miniature filters with integrated lumped components are suitable for tunable designs, but they generally suffer from high insertion loss due to the low Q of the conventional lumped components such as metal–insulator–metal (MIM) capacitors and planar inductors.

This paper investigates the application of microelectromechanical system (MEMS) capacitors as the integrated tuning elements of miniature bandpass filters in the microwave band. MEMS capacitors are high-Q elements ($>$300 at 21 GHz) and when used for loading the resonators of a coplanar waveguide (CPW) filter, they add little to the midband insertion loss. A number of researchers have successfully used MEMS capacitors to implement low-loss tunable filters [14]–[17]. The reported MEMS filters typically show a lower insertion loss compared to the semiconductor-based counterparts [18]–[20], but they are relatively poor in terms of the tunability.

In this study, we use MEMS bridges to periodically load portions of the CPW resonators in a familiar filter topology based on half-wave resonators. The partial loading of the resonators serves to reduce size in that: 1) it forms a slow-wave structure with a high effective propagation constant and 2) the partial loading configuration lowers the characteristic impedance of the CPW line in the area where the energy storage is predominantly capacitive, resulting in a smaller required electrical length at resonance. In the tunable version, the MEMS bridges are actuated by applying a dc bias, resulting in a voltage-controlled loading and a tunable passband. The tunable filter tunes over a 14% bandwidth from 18.6 to 21.4 GHz with minimal variations in the fractional bandwidth and passband response. A nonlinear study of the miniature tunable filter is presented in Section IV.

II. Slow-Wave MEMS Resonators and Miniature Filter

A. Periodic Loading of CPW Resonators

Fig. 1 presents a MEMS bridge capacitor and its equivalent circuit model [21]. The finite width of the bridge (w) and the current path over the bridge result in a phase delay that is taken into account by adding certain line lengths $(w + \Delta l)/2$ to the model. Typically, L is around 10 pH, and when the frequency of operation is far below the self resonance of the bridge, one may absorb its reactive effects in C. MEMS capacitive bridges may be used to periodically load transmission lines and form a slow-wave structure with a high effective dielectric constant and

Manuscript received January 17, 2003; revised March 28, 2003. This work was supported by the National Science Foundation under Contract ECS-9979428.

A. Abbaspour-Tamijani and G. M. Rebeiz are with the Department of Electrical Engineering and Computer Science, Radiation Laboratory, The University of Michigan at Ann Arbor, Ann Arbor, MI 48109-2122 USA (e-mail: abbasa@engin.umich.edu; rebeiz@umich.edu).

L. Dussopt was with the Department of Electrical Engineering and Computer Science, The University of Michigan at Ann Arbor, Ann Arbor, MI 48109-2122 USA. He is now with CEA-Leti, 38054 Grenoble, France (e-mail: laurent.dussopt@cea.fr).

Digital Object Identifier 10.1109/TMTT.2003.814317

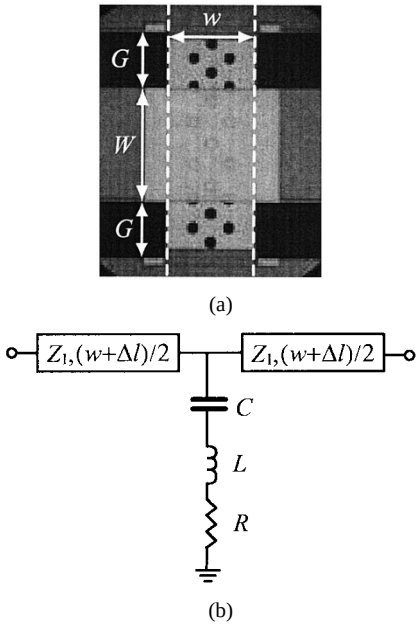

Fig. 1. MEMS varactor over a CPW line. (a) Photograph: dashed lines show the reference planes. (b) Circuit model.

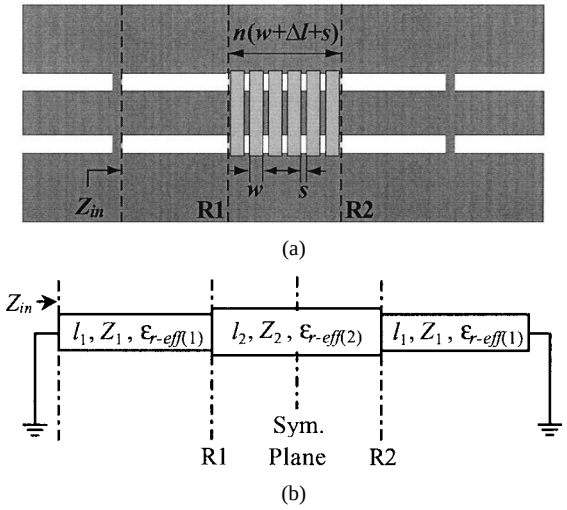

Fig. 2. MEMS slow-wave resonator. (a) Short-ended half-wave resonator with $n = 6$ bridges. (b) Circuit model.

a low characteristic impedance. The loaded section may be modeled by cascading the T-equivalent networks of the individual bridges and the intermittent line segments, or by using a simple loaded line model, as proposed in [22]. In the latter case, however, the loading period must be defined to include the bridge widths w and the correction lengths Δl for accurate results.

Fig. 2(a) presents a MEMS slow-wave section consisting of six bridges in the middle of a short-ended half-wave CPW resonator. The circuit model is presented in Fig. 2(b). Z_1 and $\varepsilon_{r-\text{eff}(1)}$ are the characteristic impedance and effective dielectric constant of the unloaded CPW line. If n is the number of bridges (in a general case) and s is the edge-to-edge separation

TABLE I
MEASURED PARAMETERS OF THE STANDARD AND LOADED T-LINE RESONATORS

Resonator Type	f_0 (GHz)	Length ($\lambda_g@f_0$)	Resonator Q	MEMS Bridge Q*
Standard	24.3	0.5	62	–
w/ 6-bridge loading	21.0	0.163	56	400
w/ 8-bridge loading	21.0	0.145	48	400

*Extracted value using model.

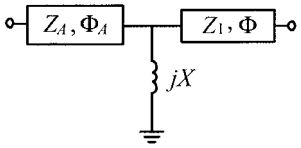

Fig. 3. Inductive realization of the impedance inverter.

between the bridges, then l_2, Z_2, and $\varepsilon_{r-\text{eff}(2)}$ of the loaded section are given by

$$l_2 = n(s + w + \Delta l)$$
$$Z_2 = \frac{Z_1}{\sqrt{K}}$$
$$\varepsilon_{r-\text{eff}(2)} = K\varepsilon_{r-\text{eff}(1)}$$

where

$$K = 1 + \frac{cZ_1C}{(s + w + \Delta l)\sqrt{\varepsilon_{r-\text{eff}(1)}}}$$
$$c = 3 \times 10^8 \text{ m/s} \quad (1)$$

In a practical design, K can be quite large (20–50).

Partial loading of the CPW resonator around the voltage maximum proves to be very effective in reducing the resonance length. There are two different effects involved in miniaturization: the slow phase velocity over the loaded region, and the step impedance configuration. The design equations for the slow-wave MEMS resonator are derived from the model in Fig. 2(b) by replacing the symmetry plane with a magnetic wall and using the resulting half-circuit

$$\overline{Z}'_{in} = j\overline{X}'_{in} = j\frac{\tan\vartheta_1 - \overline{Z}_2\cot\vartheta_2}{1 + \overline{Z}_2\tan\vartheta_1\cot\vartheta_2} \quad (2)$$

where ϑ_1 and ϑ_2 are the electrical lengths corresponding to l_1 and $l_2/2$, respectively, and the prime sign refers to the half-circuit. The bar sign indicates normalization to the characteristic impedance of the unloaded transmission line Z_1. The short-ended resonator forms a series resonance at the input with the corresponding resonance condition expressed as

$$\tan\vartheta_1 - \overline{Z}_2\cot\vartheta_2 = 0 \quad (3)$$

The reactance slope of this resonator is given by

$$\overline{x} = 2\overline{x}' = \omega_0\left.\frac{\partial\overline{X}'_{in}}{\partial\omega}\right|_{\omega=\omega_0} = \vartheta_1 + \vartheta_2\cos^2\vartheta_1\csc^2\vartheta_2. \quad (4)$$

Equations(3) and (4) form the basis for design of filters using slow-wave MEMS resonators.

Table I provides a quantitative comparison between two slow-wave MEMS resonators with six and eight MEMS bridges and a standard short-ended CPW resonator. All resonators are based on 3-μm-thick electroplated gold with dimensions of 80/160/80 μm (*G/W/G*) on a 500-μm-thick

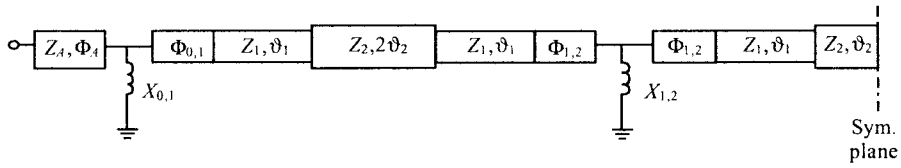

Fig. 4. Complete circuit model for the miniature three-pole filter (only one-half of the circuit is shown).

quartz wafer with $\varepsilon_r = 3.8$ and $\tan\delta = 0.0002$. The dimensions of the CPW line are chosen to minimize the conductor losses, as per [23]. The measured CPW line parameters are $Z_1 = 77\ \Omega$ and $\varepsilon_{r-\mathrm{eff}(1)} = 2.37$, and the attenuation constant is $\alpha_1 = 0.37$ dB/cm at 21 GHz. The MEMS bridges are fabricated using electroplated gold membranes at an average height of 1.1 μm above the center conductor of the CPW line ($w = 50\ \mu$m, $s = 20\ \mu$m). The simulated values[1] of C and Δl are 74 fF and $-20\ \mu$m, respectively, which corresponds to $K = 23.2$ according to (1).

The measured unloaded Q's and lengths of the resonators are given in Table I. The lengths are normalized to the guided wavelength of the unloaded CPW line at the respective resonant frequencies. The slow-wave resonators are more than three times shorter than the standard resonator and show considerable miniaturization. This generally entails a much smaller quality factor. However, the MEMS capacitors used in this case are high-Q elements with an estimated Q of 350–450 at 21 GHz ($R \approx 0.25 \pm 0.05\ \Omega$) [24], and the loading of the resonator reduces Q by only 10%–20%.

B. MEMS Miniature Filter

A bandpass filter may be designed by coupling of the slow-wave MEMS resonators through inductive impedance inverters. An inductive impedance inverter is the T combination of a shunt inductor and two series negative transmission-line lengths. In the general case, shown in Fig. 3, when the CPW line comprising the resonator has a characteristic impedance different from that of the input/output line (here, 77 Ω versus 50 Ω), the design equations are

$$\begin{aligned} \overline{X} &= \left[(\overline{K}^2 - 1)\overline{Z}_A^{-2} + (\overline{K}^{-2} - 1)\right]^{(-1/2)} \\ \Phi_A &= \frac{(p+q)}{2} \\ \Phi &= \frac{(p-q)}{2} \\ p &= -\tan^{-1}\left(\left(\overline{Z}_A^{-1} + 1\right)\overline{X}\right) \\ q &= -\tan^{-1}\left(\left(\overline{Z}_A^{-1} - 1\right)\overline{X}\right) \end{aligned} \tag{5}$$

where $\overline{Z}_A$ is the characteristic impedance of the input/output transmission line and the bar sign indicates normalization to the unloaded CPW line Z_1. For $\overline{Z}_A = 1$, these equations reduce to the standard formulas in [25].

In the CPW design, the shunt inductors are realized using narrow inductive lines between the center conductor and ground plane [26]. For larger values of inductance, the lines are extended inside the ground conductors (see Figs. 4 and Figs. 5), forming short-circuited high-impedance CPW stubs. However, the cuts in the ground conductor introduce parasitic series inductances that are included in the model by adding correction lengths to the individual arms of the inverters. To avoid anomalies in the asymmetric inductive stubs at the input and output, the ground path is closed using air-bridges that are fabricated in the same process along with the MEMS capacitors. Several shunt inductors were individually fabricated and tested. The measured values of inductance for all of the examined cases were 10%–20% lower than the predicted values using commercial method of moments (MoM) simulators.[2]

TABLE II
MODEL PARAMETERS FOR THE 21-GHz MINIATURE FILTER WITH SIX-BRIDGE LOADING

$Z_A(\Omega)$	50	$L_{0,1} = L_{3,4}$ (pH)	135
$Z_1(\Omega)$	77	$L_{1,2} = L_{2,3}$ (pH)	36
$Z_2(\Omega)$	15.9	$\Phi_{0,1} = \Phi_{3,4}$ (deg.)	−11.6
ϑ_1 (deg.)	21.2	$\Phi_{1,2} = \Phi_{2,3}$ (deg.)	−3.5
ϑ_2 (deg.)	28.0	Φ_A (deg.)	−18.7

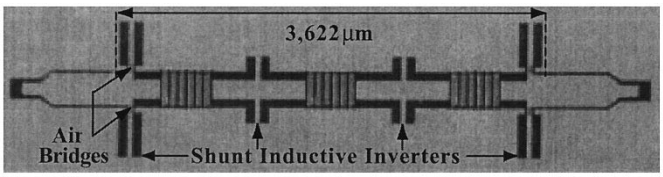

Fig. 5. Photograph of the fabricated MEMS miniature filter (design #1 in Table III).

Fig. 4 shows the complete circuit model of the miniature filter. This model has been used to design a three-pole Chebyshev filter with 8% equiripple bandwidth centered at 21 GHz and 0.05-dB passband ripple. The filter is based on the slow-wave MEMS resonators with six bridges (Table I). The model parameters for this design are given in Table II. In the physical layout, the unloaded sections of the resonators are adjusted to accommodate the correction lengths of the inductive stubs.

The fabricated miniature filter is shown in Fig. 5. The total length of the miniature filter is 3620 μm, which is only 0.39 λ_g at 21 GHz ($\lambda_g = 9280\ \mu$m). A standard filter without the bridges would have been 12 560-μm long (3.5 times longer). Fig. 6 presents the simulated and measured S-parameters of the miniature filter. The measured passband is centered at 21.1 GHz. The measured midband insertion loss is 2.9 dB versus the simulated value of 2.3 dB, neglecting the loss in the MEMS capacitors. The 1-dB fractional bandwidth is 8.6%. Further miniaturization may be obtained using more bridges on each resonator at the expense of higher midband insertion loss. A second design based on the eight-bridge slow-wave resonators (Table I)

[1]*Advanced Design System 2002*, Agilent Technol., Santa Clara, CA, 2002.

[2]Agilent's *Advanced Design System 2002*; and *Sonnet EM Suite*, Sonnet Software Inc., Liverpool, NY, 1998.

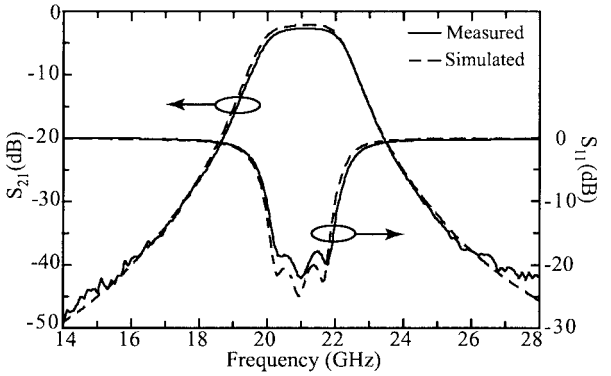

Fig. 6. Measured and simulated S-parameters of the miniature three-pole filter (design #1 in Table III).

resulted in 3.5-dB midband insertion loss. This is due to the slightly lower Q of the resonators with longer slow-wave section (see Table I). The measured data for the miniature filters with six and eight bridges per resonator are summarized in Table III.

Although the slow-wave MEMS miniature filter easily achieves a low-loss miniaturization, it suffers from sensitivity to the fabrication errors. With the state-of-the-art technology, the MEMS bridges may be fabricated with ± 0.2 μm height variations. The circuit model in Fig. 4 may be used to perform a sensitivity analysis versus the height variations. Table IV shows simulated values of the bridge capacitor, as well as the passband center frequency, and fractional 1-dB bandwidth of the slow-wave miniature filter (Design #1 of Table III) for five different values of the bridge height. At 1.1 μm, the slope of the variation of f_0 versus g is 0.734 GHz/0.1 μm. The value of the bridge capacitor used at $g = 1.1$ μm is 76 fF, which is determined by fitting the model of Fig. 4 to the measured results. This is very close to the full-wave simulated value of 74 fF used in the filter design. The fractional bandwidth Δf is virtually insensitive to the height variations. While S_C^{f0} (sensitivity of f_0 to C) is nearly constant, S_g^{f0} (sensitivity of f_0 to g) is higher at low heights since $\delta C \sim -\delta g/g^2$. Therefore, a more robust design may be obtained by using higher MEMS bridges. However, this will reduce the amount of loading and K in the slow-wave section, resulting in a lesser miniaturization.

III. Miniature Tunable Filter

The tunable filter is obtained by replacing the fixed bridge capacitors with MEMS varactors in the miniature filter presented in design #1 of Table III. Fig. 7(a) shows six MEMS varactors on the loaded section of the CPW line. The pull-down electrodes are 60-μm long and are located in the CPW gaps near the bridge anchors. To increase the capacitance ratio of the varactors, a step profile is used [27], which is higher at the pull-down areas and lower in the middle section [see Fig. 7(b)]. To reduce the ohmic losses, the bridge is electroplated with 2-μm gold, except above the pull-down electrodes. This ensures a flexible membrane with a reasonable spring constant.

The tunable filter was fabricated on a glass substrate (quartz substrates were not available) with $\varepsilon_r = 4.6$ and $\tan\delta = 0.006$, and with the same layout shown in the previous section (Fig. 5). The measured parameters of the unloaded CPW line in this

TABLE III
Measured Parameters of the MEMS Miniature Filters

	#1	#2
No. of Bridges per Resonator	6	8
Total Length (μm)	3,622	3,254
Center Frequency (GHz)	21.1	21.2
1-dB Bandwidth (%)	8.6	7.8
Insertion Loss (dB)	2.9	3.5
Ave. Bridge Height (μm)	1.1	1.1
Effective Loading Length l_2 (μm)	300	400
$\varepsilon_{r-eff(2)}$ in the Loading Region	55.0	55.0
Z_2 in the Loading Region (Ω)	15.9	15.9

TABLE IV
Simulated Passband Parameters of the MEMS Miniature Filter for Different Bridge Heights

Bridge Height g (μm)	0.9	1.0	1.1	1.2	1.3
Bridge Capacitance C (fF)	90	82	76	70	66
Center Frequency f_0 (GHz)	19.41	20.33	21.11	21.82	22.52
1-dB Bandwidth (%)	9.0	9.0	9.0	9.1	8.9

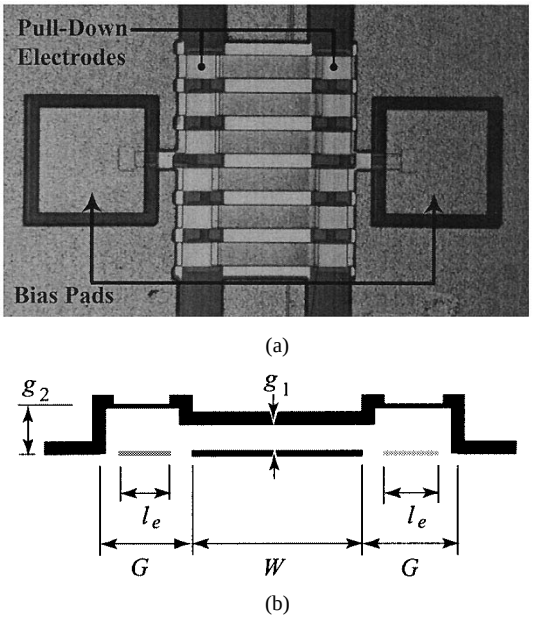

Fig. 7. Tunable load section with six varactors. (a) Photograph. (b) Bridge profile.

case are $Z_1 = 76\ \Omega$, $\varepsilon_{\text{eff}(1)} = 2.72$, and $\alpha_1 = 0.7$ dB/cm. The MEMS bridges are fabricated at the height of 1.2 μm above the CPW center conductor (g_1) instead of 1.1 μm in the quartz-based design, which compensates for the higher dielectric constant. The pull-down electrodes are fabricated using a 1000-Å-thick SiCr layer with a resistivity of 1–2 kΩ/square. The electrodes on each side of the center conductor are tied to a different bias pad to eliminate any crossover with the CPW center conductor and, therefore, minimizing the loading effects at microwave frequencies. This filter is tuned by applying a bias voltage of 0–80 V. The bridges collapse at higher applied voltages.

Fig. 8 presents the measured and simulated S-parameters of the miniature tunable filter for $V_b = 0$ V and 80 V. The exact value of the bridge height and capacitance versus the bias voltage cannot be calculated using simple formulas due

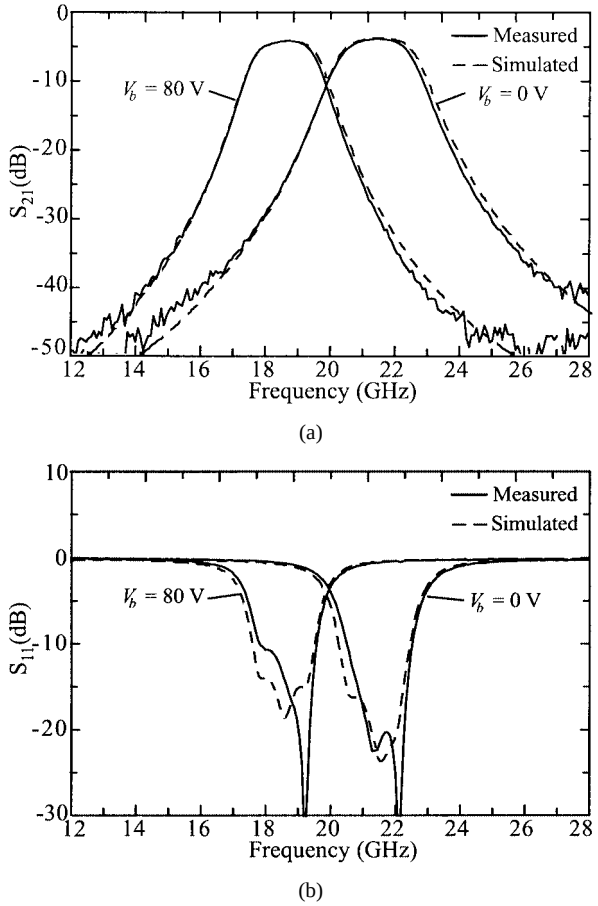

Fig. 8. Measured and simulated S-parameters of the miniature tunable filter for $V_b = 0$ and 80 V. (a) S_{21}. (b) S_{11}.

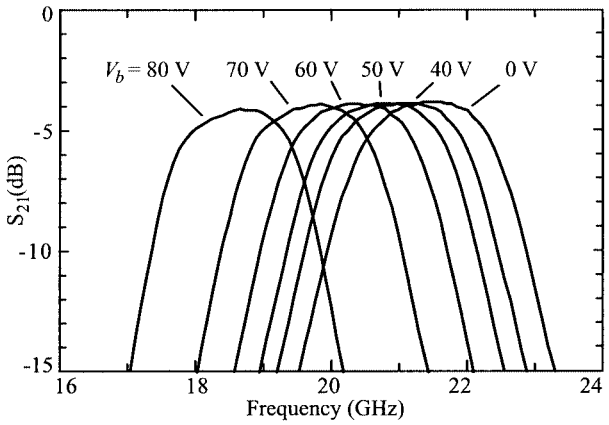

Fig. 9. Passband response of the miniature tunable filter for different values of V_b.

TABLE V
MEASURED PARAMETERS OF THE MINIATURE TUNABLE FILTER FOR DIFFERENT VALUES OF BIAS VOLTAGE

Bias Voltage (V)	0	40	50	60	70	80
Center Frequency (GHz)	21.44	21.04	20.74	20.32	19.72	18.60
Bandwidth 1-dB (%)	7.37	7.60	7.52	7.67	7.35	7.58
Insertion Loss (dB)	3.85	3.90	3.90	3.92	3.94	4.15
Bridge Capacitance (fF)*	69	71	74	77	83	93
Bridge Height (μm)*	1.20	1.17	1.12	1.08	1.00	0.89

*Fitted values based on the measurement.

to the complex mechanical structure of the stepped-profiled bridge. The simulated S-parameters are based on the model in Fig. 4 with CPW line parameters and electrical lengths replaced by the new values based on $K = 25.3 (C = 69$ fF) and $K = 45 (C = 93$ fF) for $V_b = 0$ and 80 V, respectively. The passband center frequency shifts from 21.44 GHz at 0 V to 18.60 GHz at 80 V, while the fractional bandwidth remains constant at 7.5±0.1%. The tuning range of this filter is ±7% centered at 20.0 GHz. The midband insertion loss varies from 3.85 dB in the upper band to 4.15 dB in the lower band. The higher value of loss as compared to the fixed miniature filter is believed to be due to the relatively high losses in the glass substrate. If the attenuation constant of the unloaded CPW line is changed from 0.70 dB/cm (measured on glass) to 0.37 dB/cm (measured on quartz), the simulated insertion loss in the upper band reduces to 2.8 dB, which is comparable to that of the quartz-based miniature filter. This indicates that the MEMS varactors maintain a Q of ∼350–450 similar to the fixed bridge capacitors.

An attractive feature of the miniature tunable filter is the constant fractional bandwidth in the tuning range. This is due to the use of inductive inter-resonator couplings, which compensate for the increasingly capacitive behavior of the resonators when they are tuned toward the lower frequencies [28]. While using inductive coupling along with capacitive loading generally entails closer spurious passbands and lower rejection in the higher frequencies, in the case of the miniature tunable filter, such negative effects are not observed due to the fact that the loading has a minimal impact at the second resonance mode with a voltage null at the center of the resonators. The first spurious passband in this special design appears at $> 3f_0$.

Fig. 9 shows a close-up plot of S_{21} for several values of the bias voltage. The corresponding data are summarized in Table V. The average estimated bridge resistance is $R = 0.15 \pm 0.05\ \Omega$. R cannot be determined accurately since its small impact on the midband insertion loss can be overwhelmed by the larger effect of the errors in the CPW line attenuation. A 10% error in the value α_1 used in the model can change the estimated value of R up to 50%.

One concern about the miniature tunable filter is the high value of the control voltage. The reason for the high bias voltage in this case is the short length of the pull-down electrodes ($l_e = 60\ \mu$m) and the fact that they are located very close to the anchor points, resulting in a high effective spring constant. A solution to this problem is using the center conductor of the CPW line as the pull-down electrode. However, this requires adding large MIM capacitors in series with the coupling inductors or with the bridges in order to provide dc isolation between the center conductor and bridges. The center actuated bridges typically have lower capacitive ratios, which limits the tuning range.

IV. NONLINEAR CHARACTERIZATION

Variations in the capacitance of the MEMS bridges under the high RF drive conditions result in a nonlinear behavior in the filters consisting of MEMS capacitors. While the nonlinear effects are negligible for the MEMS miniature filter with thick

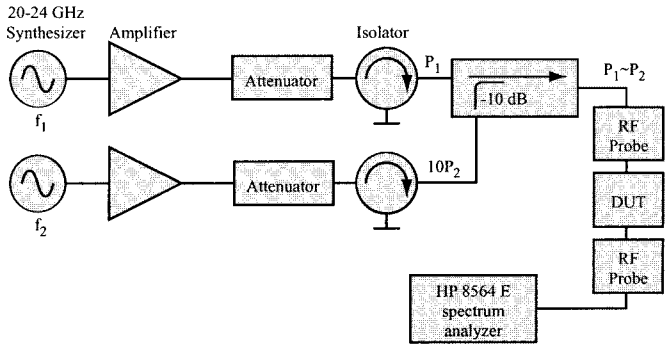

Fig. 10. Experimental setup for intermodulation measurements.

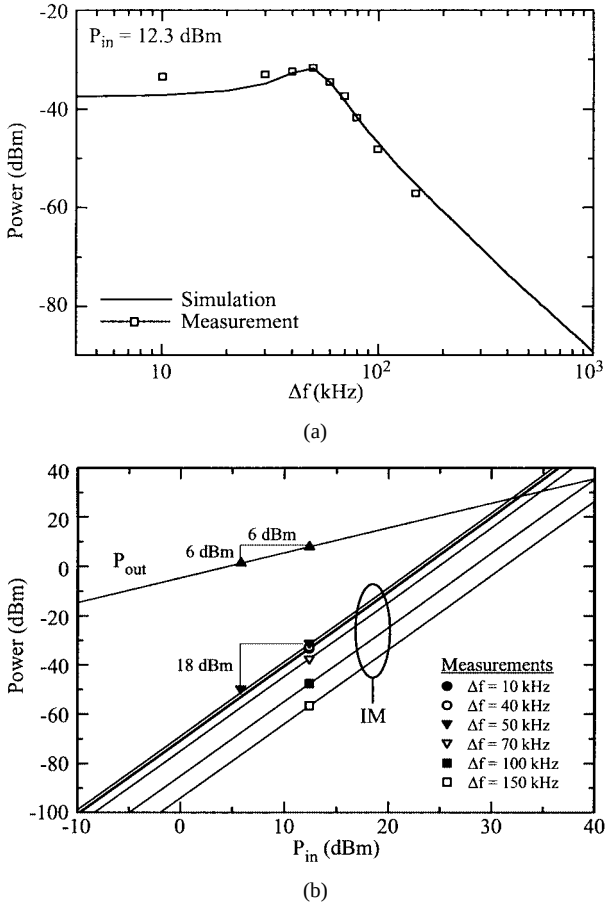

Fig. 11. Third-order intermodulation product measured at $V_b = 0$ V. (a) Two-tone IM3 versus the beat frequency. (b) Fundamental and intermodulation components versus the input power.

electroplated bridges, they should be examined more carefully in the case of the MEMS tunable filters where flexible MEMS varactors are used.

A detailed study of the nonlinear behavior of MEMS varactors and filters has been presented in [29]. This analysis shows that the nonlinear behavior of the MEMS varactor is directly related to the mechanical dynamic response of the bridge. For example, in the case of two-tone excitation, vibration of the bridge due to the force component at the beat frequency changes the capacitance, and presence of the input tones across this variable capacitor generates a third-order intermodulation. The capacitance variations and, consequently, the IM_3 products, are maximum for the beat frequency near the natural frequency of the bridge and drop quickly at larger beat frequencies.

A similar analysis can be performed on the miniature-tunable filter with slow-wave MEMS resonators. However, since the different varactors in the slow-wave sections are subject to different values of RF voltage, the analysis requires a full circuit model in which the slow-wave section is modeled by a combination of individual nonlinear MEMS varactors (18 of them) and transmission-line sections. The MEMS bridge mechanical parameters (k, Q, f_n) can be directly extracted by comparing the nonlinear model with the intermodulation measurements.

The setup used for measuring the intermodulation generation in the filter is shown in Fig. 10. The sinusoidal waveforms generated by two synthesizers are amplified, combined, and then delivered to the MEMS filter. The output power at the fundamental frequencies, as well as the third-order intermodulation products, are measured using a spectrum analyzer. Fig. 11(a) presents the measured intermodulation component (IM_3) versus the difference frequency of the input tones (Δf). The simulated curve has been generated using the nonlinear model based on the theory in [29]. The mechanical bridge parameters are adjusted to fit the measured points ($k = 190$ N/m, $Q = 1.9$, and $f_n = 52$ kHz). The high value of the spring constant is believed to be due to the very high residual stress, which is estimated around 200 MPa.

Fig. 11(b) presents the power of the fundamental and intermodulation components versus the input power for several values of the beat frequency. For $\Delta f = 50$ kHz, which is approximately equal to the bridge mechanical resonant frequency, the IIP_3 is $\sim$32 dBm. This number is typically lower for the tunable filters using diode varactors, for example, the ones in [19] ($\mathrm{IIP}_3 = 12$ dBm) and [20] ($\mathrm{IIP}_3 \leq 28$ dBm). The IIP_3 increases to $>$50 dBm for $\Delta f > 150$ kHz.

The nonlinear measurements presented here were carried out at $V_b = 0$ V. As demonstrated by Dussopt and Rebeiz [29], however, the third-order IM products vary as $1/g_0^8$, where g_0 represents the bridge height with no RF applied. Since g_0 decreases from 1.2 to 0.9 μm when the filter is tuned to 18.6 GHz (see Table V), the IM_3 level is expected to be 10 dB higher in the lower band of operation, which corresponds to a 5-dB reduction in IIP_3.

V. Conclusion

MEMS capacitors and varactors have been used to develop miniature and tunable filters at the K-band (18–22 GHz). The MEMS slow-wave resonators based on CPW lines are inductively coupled to form miniature three-pole filters, and show excellent frequency response in the passband and rejection band. The measured insertion loss is 2.9 dB at 21.1 GHz for an 8.6% MEMS miniature filter on quartz. Tunable slow-wave structures can also be used as a basis for miniature tunable filters. A tunable filter was designed using this technique and measured for different bias voltages. The center frequency tunes from 18.60 to 21.44 GHz with the passband covering 17.90–22.23 GHz. The fractional bandwidth is 7.5% over the whole tuning range. Midband insertion loss was measured at 3.85–4.15 dB. With high-Q MEMS bridges ($Q \sim 400$), the midband insertion loss of the

miniature and tunable filters are dominated by the ohmic and dielectric losses in the CPW structure, resulting in a performance comparable to the standard bandpass filters built using CPW lines.

ACKNOWLEDGMENT

The authors would like to thank T. Hancock, The University of Michigan at Ann Arbor, for performing the nonlinear measurements.

REFERENCES

[1] A. F. Sheta, K. Hettak, J. P. Coupez, C. Person, and S. Toutain, "A new semi-lumped microwave filter structure," in *IEEE MTT-S Int. Microwave Symp. Dig.*, 1995, pp. 383–386.
[2] G. L. Hey-Shipton, "Quasilumped element bandpass filters using DC isolated shunt inductors," in *IEEE MTT-S Int. Microwave Symp. Dig.*, 1996, pp. 1493–1496.
[3] E. Cristal and S. Frankel, "Hairpin-line and hybrid haipin-line/half-wave parallel-coupled-line filters," *IEEE Trans. Microwave Theory Tech.*, vol. MTT-20, pp. 719–728, Nov. 1972.
[4] J. S. Hong, M. J. Lancaster, D. Jedamzik, and R. B. Greed, "8-pole superconducting quasielliptic filter for mobile communications application," in *IEEE MTT-S Int. Microwave Symp. Dig.*, 1998, pp. 367–370.
[5] C. K. Ong, L. Chen, J. Lu, C. Y. Tan, and B. T. G. Tan, "High-temperature superconducting bandpass spiral filter," *IEEE Microwave Guided Wave Lett.*, vol. 9, pp. 407–409, Sept. 1999.
[6] J. J. Yu, S. T. Chew, M. S. Leong, and B. L. Ooi, "New class of microstrip miniaturized filter using triangular stub," *Electron. Lett.*, vol. 37, no. 19, pp. 1169–1170, 2001.
[7] J. A. Curtis and S. J. Fiedziusko, "Miniature dual mode microstrip filters," in *IEEE MTT-S Int. Microwave Symp. Dig.*, 1991, pp. 443–446.
[8] J. S. Hong and M. J. Lancaster, "Microstrip bandpass filter using degenerate modes of a novel meander loop resonator," *Microwave Guided Wave Lett.*, vol. 5, pp. 371–372, Nov. 1995.
[9] H. Yabuki, M. Sagawa, M. Matsu, and M. Makimoto, "Stripline dual-mode ring resonators and their application to microwave devices," *IEEE Trans. Microwave Theory Tech.*, vol. 44, pp. 723–729, May 1996.
[10] Z. M. Hejazi, P. S. Excell, and Z. Jiang, "Compact dual-mode filters for HTS satellite communication systems," *IEEE Microwave Guided Wave Lett.*, vol. 8, pp. 275–277, Aug. 1998.
[11] G. L. Matthaei, N. O. Fenzi, R. J. Forse, and S. M. Rohlfing, "Hairpin-comb filters for HTS and other narrow-band applications," *IEEE Trans. Microwave Theory Tech.*, vol. 45, pp. 1231–1236, Aug. 1997.
[12] W. J. Chappell, M. P. Little, and L. P. B. Katehi, "High isolation, planar filters using EBG substrates," *IEEE Microwave Wireless Comp. Lett.*, vol. 11, pp. 246–248, June 2001.
[13] X. Gong, W. J. Chappell, and L. P. B. Katehi, "Capacitive defect EBG resonators," in *IEEE MTT-S Int. Microwave Symp. Dig.*, 2002, pp. 1091–1094.
[14] D. Peroulis, S. Pacheco, K. Sarabandi, and L. Katehi, "Tunable lumped components with applications in reconfigurable MEMS filters," in *IEEE MTT-S Int. Microwave Symp. Dig.*, 2001, pp. 341–344.
[15] Y. Liu, A. Borgioli, A. S. Nagra, and R. A. York, "Distributed MEMS transmission lines for tunable filter applications," *Int. J. RF Microwave Computer-Aided Eng.*, vol. 11, pp. 254–260, Aug. 2001.
[16] A. Abbaspour-Tamijani, L. Dussopt, and G. M. Rebeiz, "A millimeter-wave tunable filter using MEMS varactors," in *Eur. Microwave Conf. Dig.*, Milan, Italy, Sept. 2002, pp. 813–815.
[17] E. Fourn, A. Pothier, C. Champeaux, P. Tristant, A. Catherinot, P. Blondy, G. Tanne, E. Rius, C. Person, and F. Huret, "MEMS switchable interdigital coplanar filter," *IEEE Trans. Microwave Theory Tech.*, vol. 51, pp. 320–324, Jan. 2003.
[18] I. C. Hunter and J. D. Rhodes, "Electronically tunable microwave bandpass filters," *IEEE Trans. Microwave Theory Tech.*, vol. 30, pp. 1354–1360, Sept. 1982.
[19] S. R. Chandler, I. C. Hunter, and J. C. Gardiner, "Active varactor tunable bandpass filter," *IEEE Microwave Guided Wave Lett.*, vol. 3, pp. 70–71, Mar. 1993.
[20] A. R. Brown and G. M. Rebeiz, "A varactor-tuned RF filter," *IEEE Trans. Microwave Theory Tech.*, vol. 48, pp. 1157–1160, July 2000.
[21] J. B. Muldavin and G. M. Rebeiz, "High isolation MEMS shunt switches—Part 1: Modeling," *IEEE Trans. Microwave Theory Tech.*, vol. 48, pp. 1045–1052, May 2000.
[22] R. E. Collin, *Foundations for Microwave Engineering*, 2nd ed. New York: McGraw-Hill, 1992.
[23] K. C. Gupta, R.Ramesh Garg, I.Inder Bahl, and P.Prakash Bhartia, *Microstrip Lines and Slotlines*, 2nd ed. New York: Artech House, 1996.
[24] J. S. Hayden and G. M. Rebeiz, "Very low-loss distributed X-band and Ka-band MEMS phase shifters using metal–air–metal capacitors," *IEEE Trans. Microwave Theory Tech.*, vol. 51, pp. 309–314, Jan. 2003.
[25] G. L. Matthaei, L. Young, and E. M. T. Jones, *Microwave Filters: Impedance-Matching Networks, and Coupling Structures*. New York: McGraw-Hill, 1964.
[26] J. K. A. Everard and K. K. M. Cheng, "High performance direct coupled bandpass filters on coplanar waveguide," *IEEE Trans. Microwave Theory Tech.*, vol. 41, pp. 1568–1573, Sept. 1993.
[27] L. Dussopt and G. M. Rebeiz, "High-Q millimeter-wave MEMS varactors: extended tuning range and discrete-position designs," in *IEEE MTT-S Int. Microwave Symp. Dig.*, 2002, pp. 1205–1208.
[28] G. L. Matthaei, "Narrow-band, fixed-tuned, and tunable bandpass filters with zig–zag hairpin-comb resonators," *IEEE Trans. Microwave Theory Tech.*, vol. 51, pp. 1214–1219, Apr. 2003.
[29] L. Dussopt and G. M. Rebeiz, "Intermodulation distortion and power handling in RF MEMS switches, varactors and tunable filters," *IEEE Trans. Microwave Theory Tech.*, vol. 51, pp. 1247–1256, Apr. 2003.

Abbas Abbaspour-Tamijani (S'00) received the B.S. and M.S. degrees in electrical engineering from the University of Tehran, Tehran, Iran, in 1994 and 1997, respectively, and is currently working toward the Ph.D. degree in electrical engineering with emphasis on applied electromagnetics and RF circuits at The University of Michigan at Ann Arbor.

From 1997 to 1999, he was an RF and Antenna Engineer in the telecommunication industry. During the 1999–2000 academic year, he was a visitor with the Antenna Laboratory, University of California at Los Angeles (UCLA), where he was involved with the design of feed systems for space-borne reflector antennas. In Fall 2000, he joined the Radiation Laboratory, The University of Michigan at Ann Arbor. His research area includes RF MEMS and components, phased arrays and focal plane scanning systems, and integrated front-ends.

Laurent Dussopt (S'00–A'01–M'03) received the M.S. and Agrégation degrees in electrical engineering from the Ecole Normale Supérieure de Cachan, Cachan, France, in 1994 and 1995, respectively, and the Ph.D. degree in electrical engineering from the University of Nice-Sophia Antipolis, Nice-Sophia Antipolis, France, in 2000.

From September 2000 to October 2002, he was a Research Fellow with The University of Michigan at Ann Arbor, where he was involved with RF-MEMS varactors and switches and their applications to voltage-controlled oscillators (VCOs), phase shifters, and tunable networks. He is currently with CEA-LETI, Grenoble, France. He has authored or coauthored over 25 journal and conference papers and several book chapters. His research interests include RF-MEMS components and systems, planar antennas and arrays, active antennas, and oscillating antenna arrays.

Dr. Dussopt has been a reviewer of several papers for the IEEE TRANSACTIONS ON MICROWAVE THEORY AND TECHNIQUES. He was a corecipient of the 2002 Best Student Paper Award (Second Prize) presented at the IEEE Radio Frequency Integrated Circuit (RFIC) Conference.

Gabriel M. Rebeiz (S'86–M'88–SM'93–F'97) received the Ph.D. degree in electrical engineering from the California Institute of Technology, Pasadena.

He is a Full Professor of electrical engineering and computer science (EECS) at The University of Michigan at Ann Arbor. His research interests include applying microelectromechanical systems (MEMS) for the development of novel RF and microwave components and sub-systems. He is also interested in SiGe RF integrated circuit (RFIC) design, and in the development of planar antennas and millimeter-wave front-end electronics for communication systems, automotive collision-avoidance sensors, and phased arrays.

Prof. Rebeiz was the recipient of the 1991 National Science Foundation Presidential Young Investigator Award and the 1993 URSI International Isaac Koga Gold Medal Award. He was selected by his students as the 1997–1998 Eta Kappa Nu EECS Professor of the Year. In October 1998, he was the recipient of the Amoco Foundation Teaching Award, given yearly to one faculty member of The University of Michigan at Ann Arbor for excellence in undergraduate teaching. He was the corecipient of the IEEE 2000 Microwave Prize. In 2003, he was the recipient of the Outstanding Young Engineer Award of the IEEE Microwave Theory and Techniques Society (IEEE MTT-S) and a Distinguished Lecturer for the IEEE MTT-S.